UCRL-11564

University of California

Ernest O. Lawrence Radiation Laboratory

TWO-WEEK LOAN COPY

This is a Library Circulating Copy which may be borrowed for two weeks. For a personal retention copy, call Tech. Info. Division, Ext. 5545

THE KINETICS AND MECHANISM OF FINAL STAGE DENSIFICATION IN THE VACUUM HOT-PRESSING OF FINE-GRAINED ALUMINUM OXIDE

Berkeley, California

DISCLAIMER

This document was prepared as an account of work sponsored by the United States Government. While this document is believed to contain correct information, neither the United States Government nor any agency thereof, nor the Regents of the University of California, nor any of their employees, makes any warranty, express or implied, or assumes any legal responsibility for the accuracy, completeness, or usefulness of any information, apparatus, product, or process disclosed, or represents that its use would not infringe privately owned rights. Reference herein to any specific commercial product, process, or service by its trade name, trademark, manufacturer, or otherwise, does not necessarily constitute or imply its endorsement, recommendation, or favoring by the United States Government or any agency thereof, or the Regents of the University of California. The views and opinions of authors expressed herein do not necessarily state or reflect those of the United States Government or any agency thereof or the Regents of the University of California.

Research and Development

UCRL-11564

UNIVERSITY OF CALIFORNIA

Lawrence Radiation Laboratory
Berkeley, California

AEC Contract No. W-7405-eng-48

THE KINETICS AND MECHANISM OF FINAL STAGE DENSIFICATION IN THE VACUUM HOT-PRESSING OF FINE-GRAINED ALUMINUM OXIDE

Ronald C. Rossi

(Ph. D. Thesis)

July 20, 1964

THE KINETICS AND MECHANISM OF FINAL STAGE DENSIFICATION IN THE VACUUM HOT-PRESSING OF FINE-GRAINED ALUMINUM OXIDE

Contents

Abstract v

I. Introduction 1

II. Literature Discussion 1

III. Theory 5

IV. Experimental Procedure 7

A. Apparatus 7

B. Procedure 8

C. Powder Preparation 9

V. Results and Discussion 9

A. Data Analysis 9

B. Untreated Powders 11

C. Pretreated Powder 13

D. Grain Growth 15

E. General Discussion 15

VI. Summary 16

Acknowledgments 18

References 19

Table 23

Figures 24

THE KINETICS AND MECHANISM OF FINAL STAGE DENSIFICATION IN THE VACUUM HOT-PRESSING OF FINE-GRAINED ALUMINUM OXIDE

Ronald C. Rossi

Inorganic Materials Research Division, Lawrence Radiation Laboratory, and Department of Mineral Technology, College of Engineering, University of California, Berkeley, California

July 20, 1964

ABSTRACT

The kinetics of the final stage densification of fine-grained aluminum oxide has been studied by vacuum hot-pressing between 1150° and 1350°C and from 2000 to 6000 psi. The kinetics is consistent with the Nabarro-Herring creep model. The activation energy for the final stage densification is 115 kcal/mole which agrees with the activation energy for diffusion of aluminum ions. The experimentally determined activation energy for grain growth is 36 kcal/mole which agrees with the extrinsic activation energy for oxygen diffusion.

The densification process takes place by two mechanisms: particle rearrangement and diffusional creep. The extent of densification that takes place in the initial stage depends upon the amount of sliding, fragmentation, and plastic flow that occurs. The final stage of densification takes place by diffusional creep and is controlled by aluminum ion diffusion in the case of aluminum oxide.

It has been shown that gases entrapped within pores of the hot-pressed compact will produce end-point porosities. A technique is described to remove adsorbed water when this water is the source of the gas.

I. INTRODUCTION

There has recently been an increased awareness of the improved properties of some materials made possible by the use of hot-pressing as the fabrication process. This process utilizes the simultaneous application of pressure and temperature on a powder compact and is capable of achieving higher densification at lower temperatures than normal sintering methods. In addition, the lower fabricating temperatures limit grain growth without the use of inhibiting additives. With an understanding of the process mechanisms, the control of density and microstructure is potentially feasible.

There has been little agreement among investigators as to the mechanism or mechanisms that are operative during the densification process. Models for densification by a plastic flow mechanism have been proposed frequently, but evidence supporting grain-boundary sliding, particle fragmentation, and stress-enhanced diffusion have also been presented.

The purpose of the present work was to obtain sufficient information on the process mechanism from kinetic data in an effort to clarify the inconsistencies among investigations that have appeared in the literature. Additional information has been obtained as to the extent to which entrapped gas is capable of controlling the densification process.

II. LITERATURE DISCUSSION

Three densification mechanisms have been considered in the literature as possibly occurring in the hot-pressing process: (1) plastic flow presumably by dislocation glide, (2) particle rearrangement by sliding and fragmentation, and (3) diffusion enhanced by stress.

A modification of the plastic flow model for a Bingham solid derived for sintering by Mackenzie and Shuttleworth[1] was proposed by Murray et al.[2] to explain the observed behavior in hot-pressing various oxides and carbides. The Murray model substituted the applied pressure for surface tension as the driving force and, with appropriate simplifications, obtained an expression for the rate of densification.

$$\frac{d\rho}{dt} = \frac{3\sigma}{4\eta}(1 - \rho), \qquad (1)$$

where ρ is the relative fractional density, $(1 - \rho) = P$, the volume fraction porosity, σ is the applied pressure (or applied stress), and η represents the viscosity at infinite shear rate. The integral form of this equation was also found to agree with experimental data obtained by Mangsen et al.[3] on two aluminum oxides, by Vasilos[4] on powdered fused silica, by Kingery et al.[5] in liquid phase pressure-sintering of copper-bismuth, sodium chloride-water, and ice-methanol systems, and by Jaeger and Egerton[6] on potassium-sodium niobates.

The kinetics of hot-pressing beryllium oxide and aluminum oxide in one atmosphere of argon observed by McClelland[7] did not follow the equation proposed by Murray et al. Basing his derivation on the observed end-point density, McClelland modified the sintering model of Mackenzie and Shuttleworth to include a correction for the variation of the applied stress under constant load as the porosity of the compact decreases. McClelland found agreement between his modified plastic flow model and his experimental data for beryllium oxide and aluminum oxide and concluded that a plastic flow mechanism was operative. Unfortunately, McClelland did not check his rate expression with the experimental data but used as his sole data point the observed end-point density at which time the rate of densification was presumed to be zero.

Except for the experiments conducted by McClelland, the kinetics of the final stages of densification for all materials investigated followed the Murray equation. This equation, derived for a Bingham solid, presupposes that a plastic flow mechanism is operative in the densification process. However, those materials which are known to exhibit no pyroplastic behavior, e.g., potassium-sodium niobate, obey this equation from the start of hot-pressing.

Low temperature experiments were used by Felten[8] to study the initial stages of aluminum oxide densification by hot-pressing. Although no direct evidence was presented, Felten concluded that the most probable initial mechanism was particle rearrangement by sliding aided by fragmentation. The observed effects of particle size and pressure were inconsistent with a plastic flow mechanism in the initial stage of densification. After long times the kinetics obeyed the Murray expression; however, a plastic flow mechanism in the final stage of densification cannot be reconciled with the plastic flow properties of sapphire studied by Kronberg.[9]

Direct micrographic evidence for grain-boundary sliding and fragmentation was obtained by Chang and Rhodes[10] on uranium carbide hot-pressed at high pressures. Additional evidence of the role of fragmentation in the densification process was revealed by Hashimoto[11] by using CaF_2 spheres of a uniform size. Micrographic observations showed that fragmentation of fluorite spheres corresponded with the region of maximum rate of densification. The final stage of densification also followed the Murray equation.

In both works of Felten and Hashimoto the mechanisms of particle rearrangement and fragmentation were found to be operative in the initial stage of densification. Either singular or combined these mechanisms

might be expected to display rheological plastic flow behavior; however, they could not be responsible for the observed kinetics in the final stage of densification.

Using large (0.030 and 0.040 in.) single-crystal spheres of aluminum oxide, Coble and Ellis[12] have evaluated the possible contribution to densification by a dislocation-glide plastic flow mechanism. Their results show that only limited densification by plastic flow seems possible and is only likely to occur in the initial stage of densification. A stress-enhanced diffusion mechanism was proposed as being the most probable in the final stage of densification.

Hot-pressing experiments conducted by Vasilos and Spriggs[13] on magnesium oxide and aluminum oxide have been interpreted by the Nabarro-Herring[14, 15] creep model. This model related the strain rate to a diffusion coefficient by the equation

$$\dot{\epsilon} = \frac{40\, D\Omega}{k\, T\, d^2}\, \sigma_e \qquad (2)$$

where $\dot{\epsilon}$ is the strain rate (sec^{-1}), D is the diffusion coefficient (cm^2/sec), Ω represents the volume of a vacancy (cm^3), σ_e is the effective stress (dyn/cm^2), k is Boltzmann's constant (1.38×10^{-16} ergs/°K), T is the absolute temperature, and d represents the average grain diameter (cm). The activation energies for hot-pressing determined from this model were consistent with the activation energies for cation diffusion, but the diffusion coefficients were several orders of magnitude greater than for self-diffusion.

A summary of the literature shows that the kinetics for the final stage of densification has been repeatedly found to be represented by the Murray equation derived on a plastic flow model. Rheologic plastic flow

by particle rearrangement and fragmentation have been found to be initial stage mechanisms. Plastic flow by dislocation motion has been shown to be capable of contributing only slightly to the initial stage densification of aluminum oxide and to be inconsistent with known dislocation behavior in the final stage of densification. In addition, acceptance of such a mechanism in final stage densification would require the motion of dislocations in those materials for which dislocation motion has not been observed. Interpretation of densification kinetics by a diffusional creep model has given activation energies consistent with those from self-diffusion but having diffusion coefficients several orders of magnitude greater.

III. THEORY

The identical kinetics for final stage densification observed for all materials suggests that the same single mechanism is responsible in every case. Sufficient evidence exists in the literature to eliminate both particle rearrangement and plastic flow mechanisms as the responsible mechanism. The agreement with self-diffusion activation energies suggests that final stage densification is a diffusion-controlled process and may possibly be defined by the Nabarro-Herring model.

The conditions present in hot-pressing make such a model appear attractive for the final stage of densification. The applicability of this model requires suitable corrections to account for those conditions unique in hot-pressing. Both the effect of porosity on the applied stress and the effect of die-wall constraint on the creep rate must be taken into account.

The effect of porosity on the applied stress is to increase the stress in the vicinity of the pores. Possible corrections for the effect of porosity on creep have been discussed in the literature.[16] For low porosity the

resultant effective stress, σ_e, can be related to the applied stress, σ, by the expression

$$\sigma_e = \sigma(1 + bP), \tag{3}$$

where P is the porosity and b is a stress concentration factor. An appropriate value for b can be obtained from the data of Spriggs and Vasilos[17] which give the stress concentration factor for the effect of porosity on the strength of aluminum oxide in the low porosity range. If it is accepted that the effective stress necessary to propagate a crack is independent of the amount of porosity over a narrow porosity range, their data then show that a pore is capable of affecting the applied stress by a factor of six.

The other consideration that must be taken into account is the effect of die-wall constraint on the creep rate. In unconstrained creep, a longitudinal displacement will induce a lateral displacement in which the volume change in the two displacements are equal. However, in constrained creep an increment of longitudinal displacement as a result of an applied stress will induce an increment of lateral displacement that will also induce a lateral stress equal and opposite to the longitudinally applied stress. The result is a cessation of further creep as it must be in the case of the densification process by hot-pressing at zero porosity. The stress correction factor in Eq. (3) becomes (1 + bP - 1) and Eq. (2) becomes

$$\dot{\epsilon} = \frac{\alpha}{d^2} \sigma bP , \tag{4}$$

where $\alpha = \frac{40 D\Omega}{k T}$, a constant at any temperature.

In interpreting densification data it is more convenient to express deformation by the rate of change of relative density rather than by strain

rate. The relationship between strain rate and densification rate is found by differentiating the relative density with respect to time

$$\frac{d\rho}{dt} = \frac{d\left(\frac{W/A\ell}{\rho_{th}}\right)}{dt} = \rho\left(-\frac{d\ell}{\ell dt}\right), \qquad (5)$$

where W equals the weight of the compact, A is the area and ℓ is the thickness of the compact and ρ_{th} represents the theoretical density. Since $\dot{\epsilon} = \left(-\frac{d\ell}{\ell dt}\right)$, where the minus sign denotes an increase in strain with a decrease in length, the substitution of strain rate from Eq. (4) gives the rate of densification as

$$\frac{d\rho}{dt} = \frac{\alpha}{d^2} b\,\sigma\,(P - P^2)\,. \qquad (6)$$

Neglecting the squared term for low values of porosity and substituting again for porosity gives

$$\frac{d\rho}{dt} = \frac{\alpha}{d^2} b\,\sigma\,(1 - \rho) \qquad (7)$$

in which the similarity to Eq. (1) is immediately apparent.

The observance of first-order rate kinetics for the final stage densification may indicate a diffusional creep process and a plastic flow mechanism no longer needs to be presumed.

IV. EXPERIMENTAL PROCEDURE

A. Apparatus

The fine-grained aluminum oxide used in this investigation was Linde A (0.3μ) which contains approximately 300 ppm total impurities. Pressings were made in 1 in. i.d. graphite dies in a vacuum hot-press shown schematically in Fig. 1. The dies were heated by radiation from a resistance-heated molybdenum coil. Temperature was sensed and

controlled with a Pt-Pt 10% Rh thermocouple placed within the die and protected from the graphite by a tantalum shield. The control thermocouple was calibrated over the desired temperature range with a thermocouple placed along the axis of the die so that the bead was in the position of the compact. The precision and control of temperature was estimated to be within ± 3° C.

Pressure was applied to the compact through a pneumatic-hydraulic system that could be controlled to within 1% of the gauge pressure setting. The pressure system was calibrated with a strain gauge which itself was calibrated on a dead-load, low-friction stress apparatus. Corrections were made for the influence of the atmospheric pressure on the moveable ram and for friction in the hydraulic jack.

The deformation of the compact was recorded continuously with a linear variable differential transformer and periodically checked with a dilatometer. Both instruments could be estimated to 0.0001 in.

B. Procedure

The hot-press was allowed to evacuate for various periods of time from 24 h to 4 days. The initial heating rate was 12° C/min to 800° C at which time temperature increase was arrested for 15 min to allow time to regain vacuum lost in heating. About 1 min before temperature was increased further, full pressure was applied to the compact. From 800° C to the control temperature the rate of heating was 100° C/min under fully applied load.

Time zero was taken when the compact reached the control temperature. The hot-pressing runs were either $3\frac{1}{2}$ or 5 h long. The temperature range investigated was from 1150° C to 1350° C and the pressure range was from 2000 to 6000 psi.

C. Powder Preparation

Two powder conditions were used. The first condition used as-received powder which was loaded into the die in the usual manner and cold compacted under 2000 psi. The die was then loaded into the hot-press in preparation for a pressing run.

The nominal size of the hot-pressed compacts was 1 in. in diam, 0.20 in. in height, and the weight was about 10.0 g.

The second powder condition employed a pretreatment of the powder before loading into a die. A preweighed amount of powder was immersed in isopropyl alcohol and allowed to dry in a vacuum chamber for at least 40 h. The dry powder was loaded into the die in a dry atmosphere of helium. The loaded die was prepressed at 2000 psi in air and immediately loaded into the hot-press and evacuated. The time in which the die was exposed to the air was usually from 3 to 5 min. The hot-pressing runs were conducted in the same manner for both powder conditions except that the runs for the untreated powder were $3\frac{1}{2}$ h in length, whereas all the runs were 5 h long for the pretreated powder. The time difference was a result of a change in the kinetic rate.

Electron micrographs were made from each of the hot-pressed compacts. Grain size measurements were made by a linear traverse technique in which a minimum traverse length of 100μ was used for any one compact.

V. RESULTS AND DISCUSSION

A. Data Analysis

The final density of the compact was determined by its weight and its volume which was measured by a displacement method in ethanol with

an analytic balance. To minimize error, the relative density of every compact was calculated with respect to a sapphire crystal that was measured at the same time as the compact. The maximum error in the relative density was estimated to be 0.03%; the measured reproducibility was less than 0.03%.

From the final density of the compact and the deformation curve obtained from the linear variable differential transformer, the relative density at any time was calculated and plotted. The rate of densification was determined by taking slopes from the relative density vs time plot using a prism technique.

The theoretical expression for the densification rate can then be checked with the experimentally determined data. If $m = \frac{\alpha}{d^2} b\sigma$, Eq. (7) can be written as

$$\frac{d\rho}{dt} = m(1 - \rho) \tag{8}$$

and integrated to give

$$\ln(1 - \rho) = -mt + \ln(1 - \rho_o) \tag{9}$$

where ρ_o is the relative density at time zero. Substituting porosity for relative density gives

$$\ln P = -mt + \ln P_o \tag{10}$$

which can be differentiated and, realizing that $-\frac{d\rho}{dt} = \frac{dP}{dt}$, gives

$$\ln \frac{d\rho}{dt} = -mt + \ln mP_o . \tag{11}$$

The value m can be determined independently from the slope of Eqs. (10) and (11) as well as from the ratio of their intercepts. A direct plot of Eq. (8) also gives the value of m.

B. Untreated Powders

The untreated powders were hot-pressed at 1250°C, 3000 psi, and under various operational conditions. The final stage densification kinetics obtained from these pressing runs fit Eq. (11), but the integrated form did not fit Eq. (10). When the densification rate was plotted as a function of porosity per Eq. (8), the line did not extrapolate to the origin but intercepted the abscissa at a value of porosity, P_e, denoting an end-point porosity. Such a plot is presented in Fig. 2 for runs Nos. 13 through 18. Using the end-point porosity to modify Eq. (10) to read

$$\ln (P - P_e) = -mt + \ln P_o , \qquad (12)$$

the plotted slopes agree with the slopes obtained from Eqs. (8) and (11). The lack of reproducibility in both the final porosity after $3\frac{1}{2}$ h and the extrapolated end-point porosity is indicative of an uncontrolled parameter rather than an inherent property of the material.

Although all pressing runs were made in vacuum, it was speculated that gases could become entrapped within the die chamber because of slow effusion rates along the die wall caused by tightly fitting die plugs. The evacuation times for runs Nos. 13 through 18 varied from 24 to 96 h and had no correlation with the observed variations in the results. Subsequent pressing runs were made with time arrests at 500°C from 15 min to 8 h in order to observe whether the effusion of physically adsorbed water may be responsible for the variable results. Again no correlation could be made. The kinetic results resembled those reported in Fig. 2.

The results of run No. 24, also plotted in Fig. 2, were obtained from a pressing run using a loosely fitting die plug. The improvement in results suggested that gases could indeed be trapped within the die chamber and that their release occurred at temperatures above 500°C.

From the data of Gregg[18] on the desorption of water from aluminum oxide as a function of temperature and an assumed activation energy for desorption of 20 kcal/mole, as much as 15% of the surface of the powder may be covered with a monolayer of water at 1250°C. With increasing densification, the surface area of the powder decreases driving off water into the void space within the die chamber. With tightly fitting die plugs, this water slowly effuses from the die chamber. However, densification also closes the pores so that some of the water becomes permanently entrapped within the compact. The observed end-point porosity is evidently a result of this entrapped water. When a loosely fitting die is used, more of the water is capable of escaping before the pores close; consequently, the end-point porosity is less than when tightly fitting die plugs are used.

The surface area of Linde A powders has been measured[19] by the B.E.T. method to be 15 m^2/g. Using this value of surface area and correcting for temperature and pressure, only 2 to 5% of a monolayer of water is necessary to be responsible for the observed end-point porosities.

For comparison, run No. 34 on pretreated powder has been plotted in Fig. 2. The pretreatment is capable of effectively removing chemisorbed water; thus, the end-point porosity is not observed. Since both untreated and pretreated powder follow a first-order kinetic expression, their densification mechanism is the same, but the effective driving force for the untreated powder is reduced by P_e.

Figure 3 compares the microstructure of runs Nos. 34 and 24. All the porosity seen in the microstructure of No. 34 for pretreated powder is at triple points or along grain boundaries, whereas for No. 24,

a great amount of porosity has become entrapped within a grain and is thereby removed from an effective position for further collapse. An empty pore cannot become included within a growing grain, whereas a pore containing a gas can become enclosed.

C. Pretreated Powder

The mechanism by which the pretreatment is capable of removing water is not fully understood. Physically adsorbed water is probably removed from the powder by mass action. The means by which chemisorbed water is subsequently removed is open to speculation.

An example of the kinetics of hot-pressing pretreated powders is given in Fig. 4 for those runs conducted at 1200° C. The logarithmic relationships and their derivatives are given in Figs. 5 and 6. The parameter m was obtained from the slope of these plots and from the ratio of their intercepts. The value of m was also obtained from the slope of the densification rate as a function of porosity from Fig. 7. In contrast to the untreated powder, the extrapolated data from Fig. 7 intersect the origin for all pretreated powders.

The hot-pressing kinetics at the other temperatures are similar to those presented for 1200° C. All slopes were taken from the portion of the curve where the grain growth rate is low. Grain size measurements taken after 2 h at 1250° C and 1300° C showed that almost 90% of the grain growth observed after 5 h had occurred.

The relationship between the applied stress and md^2 is shown in Fig. 8. The slopes are equal to αb which are constants at any temperature. Diffusion coefficients were calculated from the data for each specimen and summarized with all other data in Table I.

Figure 9 is a plot of log D as a function of reciprocal temperature which gives an activation energy of 115 kcal/mole. The self-diffusion activation energy of aluminum ions in aluminum oxide has been measured as 114 kcal/mole by Paladino and Kingery.[20] The agreement is excellent and indicates that final stage densification proceeds by diffusional creep controlled by aluminum ion diffusion. The diffusion coefficients extrapolated to higher temperatures are approximately two orders of magnitude greater than self-diffusion coefficients.

The reason for larger diffusion coefficients can be speculated upon. Recent investigations have shown that cation diffusion can be enhanced at grain boundaries[21, 22] and the region of a grain that may be affected by a boundary may be as large as 10^2 - 10^4 A.[23-26] For submicron particles as used in this investigation, a very large volume fraction of a grain may be affected by a boundary. One of the possible reasons for the higher diffusion coefficients observed in this study is the enhancement of cation diffusion by an increase in the boundary layer of fine grains. The effect of grain size on cation diffusion has been observed in the case of cesium chloride where the diffusion coefficients for cesium ions increase with a decrease in grain size.[27]

Another possible reason may be the effect of porosity on the diffusion path length. The Nabarro-Herring model uses the grain radius as a measure of the diffusion path length; however, the localized stress in the vicinity of a pore is increased, and thereby the localized atomic mobility is also increased. Therefore, the diffusion path length may be much less than the grain radius. Diffusion coefficients calculated from creep data by the Nabarro-Herring model[28-30] have been greater than self-diffusion coefficients and may indicate that this model overestimates

the diffusion coefficients because of an inadequate measure of the diffusion path length.

D. Grain Growth

Examples of the grain size and microstructure of the hot-pressed compacts for pretreated powder are given in Fig. 10 for each temperature and various pressures. Apparent are the equiaxed structure and the absence of entrapped porosity.

In Fig. 11 is a plot of log $d_{(\text{after } 5\text{ h})}$ as a function of reciprocal temperature which gives an activation energy for grain growth of 36 kcal/mole. This value agrees favorably with the extrinsic activation energy for oxygen diffusion of 33-37 kcal/mole measured by Oishi and Kingery[26] on a selected group of single-crystal spheres and on polycrystalline aluminum oxide. This agreement suggests that grain growth is controlled by the mobility of oxygen at the grain boundary which is consistent with the generally accepted theory of grain growth.[31]

The activation energy for grain growth in MgO[32] has been shown to correspond with the extrinsic activation energy for oxygen,[33] while in UO_2 grain growth activation energy corresponds with the value for uranium ion.[34, 35] In each of these cases grain growth is seen to be controlled by the structure-determining ion.

E. General Discussion

The conclusion based on this study and on work reported in the literature is that the densification process takes place by two major mechanisms: particle rearrangement and diffusional creep. The very high densification rate and the high relative density that can be obtained in the initial stage of the process can only be accomplished by the

rearrangement of particles. Particle rearrangement can take place by the singular or combined mechanisms of particle sliding, fragmentation, and plastic flow by dislocation motion. It is believed that particle sliding is the main contributor to densification. The role in which fragmentation and plastic flow play in the process will depend upon the local stress experienced and the fracture strength or yield strength of the material; however, no densification is visualized by these mechanisms other than to facilitate particle rearrangement by sliding.

Very high densities have been achieved by low temperature hot-pressing of materials such as MgO which fractures easily and which can plastically deform at relatively low temperatures. Higher temperatures are needed for aluminum oxide in which the fracture strength is higher and in which only basal slip is possible at hot-pressing temperatures. Very strong materials and those exhibiting no pyroplastic behavior, such as the carbides, need hot-pressing temperatures that are often very near their melting temperature.

The final stage of densification, as has been studied in this work, is by diffusional creep described by the Nabarro-Herring model. The kinetics for this stage of densification has been observed in most investigations of hot-pressing. In hot-pressing materials such as carbides, no fragmentation or plastic flow may take place and there may be little particle sliding. Diffusional creep may be solely operative almost from the outset.

VI. SUMMARY

End-point porosities have been observed in the hot-pressing of aluminum oxide and are believed to be due to entrapped gases within pores of the compact. It has been shown that the most probable source

of the gas in this case is water adsorbed on the surface of the powder. When the powder is pretreated so as to remove adsorbed water, the powder can be hot-pressed to high density by first-order kinetics.

The final stage densification kinetics obeys the Nabarro-Herring creep model. Diffusion coefficients calculated from this model give an activation energy that agrees excellently with the activation energy for the self-diffusion of aluminum ions in aluminum oxide. The higher diffusion coefficients observed in the densification study may be a result of the effect of grain size on diffusion rates or the effect of stress on atomic mobility in the vicinity of a pore.

The activation energy for grain growth was consistent with the extrinsic activation energy for oxygen diffusion in aluminum oxide. Grain growth rate is evidently determined by the structure determining ion.

The densification process by hot-pressing takes place by two major mechanisms: the initial stage mechanism is by particle rearrangement and the final stage mechanism is by diffusional creep. Particle rearrangement occurs mainly by particle sliding which is aided by fragmentation and plastic flow. The fracture strength and yield strength of the material will determine the amount of fragmentation or plastic flow that will occur and consequently the extent of initial stage densification.

ACKNOWLEDGMENT

The author wishes to thank Professor R. M. Fulrath for his help and guidance in conducting this work. Acknowledgment is extended to R. Buehrig for the preparation of microstructures and to S. M. Copley, D. P. H. Hasselman, and Y. Oishi for many helpful suggestions.

This work was done under the auspices of the U. S. Atomic Energy Commission.

REFERENCES

1. J. K. Mackenzie and R. Shuttleworth, "Phenomenological Theory of Sintering," Proc. Phys. Soc. (London), 62 [360B] 833-52 (1949).
2. P. Murray, D. T. Livey, and J. Williams, "Hot Pressing of Ceramics"; pp. 147-71 in Ceramic Fabrication Processes, (W. D. Kingery, editor). Technology Press of Massachusetts Institute of Technology and John Wiley & Sons, Inc., New York, 1958. 235 pp.
3. G. E. Mangsen, W. A. Lambertson, and B. Best, "Hot Pressing of Aluminum Oxide," J. Am. Ceram. Soc., 43 [2] 55-59 (1960).
4. T. Vasilos, "Hot Pressing of Fused Silica," J. Am. Ceram. Soc., 43 [10] 517-19 (1960).
5. W. D.Kingery, J. M. Woulbroun, and F. R. Charvat, "Effects of Applied Pressure on Densification During Sintering in the Presence of a Liquid Phase," J. Am. Ceram. Soc., 46 [8] 391-95 (1963).
6. R. E. Jaeger and L. Egerton, "Hot Pressing of Potassium-Sodium Niobates," J. Am. Ceram. Soc., 45 [5] 209-13 (1962).
7. (a) J. D. McClelland, "Kinetics of Hot Pressing of Ceramics"; pp 157-71 in Powder Metallurgy -- Proceedings of International Conference, New York, 1960. Edited by Werner Leszynski. Interscience Publishers, New York, 1961. 847 pp.

   (b) J. D. McClelland and E. H. Zehms, "End-Point Density of Hot-Pressed Alumina," J. Am. Ceram. Soc., 46 [2] 77-80 (1963).
8. E. J. Felten, "Hot Pressing of Alumina Powders at Low Temperatures," J. Am. Ceram. Soc., 44 [8] 381-85 (1961).
9. M. L. Kronberg, "Dynamical Flow Properties of Single Crystals of Sapphire, I," J. Am. Ceram. Soc., 45 [6] 274-79 (1962).

10. R. Chang and C. G. Rhodes, "High-Pressure Hot-Pressing of Uranium Carbide Powders and Mechanism of Sintering of Refractory Bodies," J. Am. Ceram. Soc., 45 [8] 379-82 (1962).

11. Y. Hashimoto, "First-Stage Densification of CaF_2 Under Pressure Temperature," M. S. Thesis, 1964, University of California, Berkeley, California. (UCRL-11214).

12. R. L. Coble and J. S. Ellis, "Hot-Pressing Alumina -- Mechanisms of Material Transport," J. Am. Ceram. Soc., 46 [9] 438-41 (1963).

13. T. Vasilos and R. M. Spriggs, "Pressure Sintering: Mechanisms and Microstructure for Alumina and Magnesia," J. Am. Ceram. Soc., 46 [10] 493-96 (1963).

14. F. R. N. Nabarro, "Deformation of Crystals by Motion of Single Ions"; pp 75-90 in Rept. Conf. Strength of Solids (Univ. Bristol), July 1947 (published 1948).

15. Conyers Herring, "Diffusional Viscosity of a Polycrystalline Solid," J. Appl. Phys., 21 [5] 437-45 (1950).

16. R. H. Spriggs and T. Vasilos, "Fundamental Relation Between Creep Rate and Porosity for Polycrystalline Ceramics," J. Am. Ceram. Soc., 47 [1] 47 (1964).

17. R. H. Spriggs and T. Vasilos, "Effect of Grain Size on Transverse Bend Strength of Alumina and Magnesia," J. Am. Ceram. Soc., 46 [5] 225-28 (1963).

18. S. J. Gregg, "Some Observations on the Sorption of Water by Oxides"; pp 68-75 in Chemisorption. Edited by W. E. Garner, Symp. Proc. of Chem. Soc. (London) 1956, Butterworth Scientic Publ., London, 1957. 277 pp.

19. J. A. Yopps and D. W. Fuerstenau, "The Zero Point of Charge of Alpha-Alumina," J. Colloid Sci., 19 [1] 61-71 (1964).

20. A. E. Paladino and W. D. Kingery, "Aluminum-Ion Diffusion in Aluminum Oxide," J. Chem. Phys., 37 [5] 957-62 (1962).

21. J. P. Roberts and C. Wheeler, "Diffusion of Zinc in Polycrystalline Zinc Oxide," Trans. Faraday Soc., 56 [4] 570-80 (1960).

22. W. H. Rhodes and R. E. Carter, "Ionic Self-Diffusion in Calcia-Stabilized Zirconia"; presented at the Sixty-Fourth Annual Meeting, The American Ceramic Society, New York, N. Y., April 30, 1962 (Symposium on Kinetics of Ceramic Reactions, No. 1-2s-62).

23. L. W. Barr, I. M. Hoodless, J. A. Morrison, and R. Rudham, "Effects of Gross Imperfections on Chloride-Ion Diffusion in Crystals of Sodium Chloride and Potassium Chloride," Trans. Faraday Soc., 56 [449] 697-708 (1960).

24. R. H. Condit and J. B. Holt, "Oxygen Diffusion in the Grain Boundary of MgO Bicrystals"; presented at the Sixty-Sixth Annual Meeting, The American Ceramic Society, Chicago, Ill., April 21, 1964 (Symposium on Diffusion in Crystalline Solids, No. 3-4s-64).

25. B. J. Wuensch and T. Vasilos, "Grain-Boundary Diffusion in MgO," J. Am. Ceram. Soc., 47 [2] 63-68 (1964).

26. Y. H. Oishi and W. D. Kingery, "Self-Diffusion of Oxygen in Single-Crystal and Polycrystalline Aluminum Oxide," J. Chem. Phys., 33 [2] 480-86 (1960).

27. J. F. Laurent and Jacques Benard, "Self-Diffusion of Ions in Polycrystalline Alkali Halides," Phys. Chem. Solids, 7 [2-3] 218-27 (1958).

28. S. I. Warshaw and F. H. Norton, "Deformation Behavior of Polycrystalline Aluminum Oxide," J. Am. Ceram. Soc. 45 [10] 479-86 (1962).

29. R. C. Folweiler, "Creep Behavior of Pore-free Polycrystalline Aluminum Oxide," J. Appl. Phys. 32 [5] 773-78 (1961).

30. R. L. Coble and Y. H. Guerard, "Creep of Polycrystalline Aluminum Oxide," J. Am. Ceram. Soc., 46 [7] 353-54 (1963).

31. D. Turnbull, "Theory of Grain Boundary Migration Rates," Trans. A.I.M.E. 191 661-65 (1951).

32. A. U. Daniels, Jr., R. C. Lowrie, Jr., R. L. Gibby, and Ivan B. Cutler, "Observations on Normal Grain Growth of Magnesia and Calcia," J. Am. Ceram. Soc., 45 [6] 282-85 (1962).

33. Y. H. Oishi and W. D. Kingery, "Oxygen Diffusion in Periclase Crystals," J. Chem. Phys. 33 [3] 905-06 (1960).

34. J. R. MacEwan, "Grain Growth in Sintered Uranium Dioxide: I, Equiaxed Grain Growth," J. Am. Ceram. Soc., 45 [1] 37-41 (1962).

35. J. Belle, A. B. Auskern, W. A. Bostrom, and F. S. Susko, "Diffusion Kinetics in Uranium Dioxide," U. S. Atomic Energy Comm., Rept. No. WAPD- T- 1155, 25pp. (March 1960).

Table I. Summary of results for pretreated powder.

Compact No.	Temp. °C	Stress psi	$m \times 10^4$ sec^{-1}	$d \times 10^4$ cm	$md^2 \times 10^{13}$ cm^2/sec	$D \times 10^{13}$ cm^2/sec	P after 5 h
53	1150	6000	0.504	0.41	0.835	0.0786	0.0375
58	1150	6000	0.500	0.39	0.781	0.0735	0.0287
44	1200	3000	0.450	0.58	1.52	0.296	0.0593
48	1200	4000	0.587	0.59	2.04	0.299	0.0304
45	1200	5000	0.732	0.58	2.49	0.291	0.0152
49	1200	6000	1.07	0.55	3.23	0.315	0.0091
35	1250	2000	0.517	1.03	5.48	1.65	0.0498
60	1250	2000	0.412	0.94	3.60	1.09	0.0332
37	1250	2500	0.625	0.85	4.52	1.09	0.0281
34	1250	3000	0.754	0.95	6.81	1.37	0.0210
33	1250	4000	1.13	0.81	7.43	1.12	0.0103
51	1250	4000	1.06	0.89	8.39	1.27	0.0067
36	1250	5000	1.24	0,81	8.16	0.999	0.0033
54	1250	5000	1.24	0.85	9.05	1.10	0.0033
39	1300	2000	0.542	1.38	10.4	3.26	0.0225
57	1300	2500	0.889	1.31	15.3	3.83	0.0075
38	1300	3000	1.06	1.37	19.9	4.15	0.0054
50	1300	3000	1.05	1.35	19.2	4.00	0.0053
52	1300	3500	1.27	1.27	20.5	3.66	0.0026
59	1350	2000	0.758	2.06	32.2	10.4	0.0045

FIGURE LEGENDS

Fig. 1. Schematic diagram of hot press.

1. Vacuum cover
2. Top yoke
3. Load bearing column
4. Radiation shield
5. Mo heating coil
6. Sight window
7. Insulation block
8. Plunger
9. Bottom support plate
10. Vacuum port
11. Hydraulic ram
12. Extension rod
13. Linear variable differential transformer
14. Support block
15. Pressure inlet
16. Micrometer head
17. Bellows
18. Graphite plunger
19. Graphite plug
20. Powder compact
21. Graphite die
22. Thermocouple
23. Air inlet

Fig. 2. The relationship between densification rates and porosity for untreated powder at 1250°C.

Fig. 3. Microstructural comparison of compacts No. 24 from untreated powder and No. 34 from pretreated powder; both were pressed at 1250°C and 3000 psi.

Fig. 4. Density-time relationship for pretreated powder at 1200°C.

Fig. 5. Log porosity vs time for pretreated powder at 1200°C.

Fig. 6. Log densification rate vs time for pretreated powder at 1200°C.

Fig. 7. The relationship between densification rates and porosity for pretreated powder at 1200°C.

Fig. 8. The correlation between md^2 and stress for pretreated powder.

Fig. 9. Log of diffusion coefficient as a function of reciprocal temperature for the densification process.

Fig. 10. Examples of microstructures of pretreated powder at various temperatures and pressures.

a. 1150°C , 6000 psi
b. 1200°C , 5000 psi
c. 1250°C , 2500 psi
d. 1300°C , 2000 psi
e. 1350°C , 2000 psi

Fig. 11. Log of grain size as a function of reciprocal temperature.

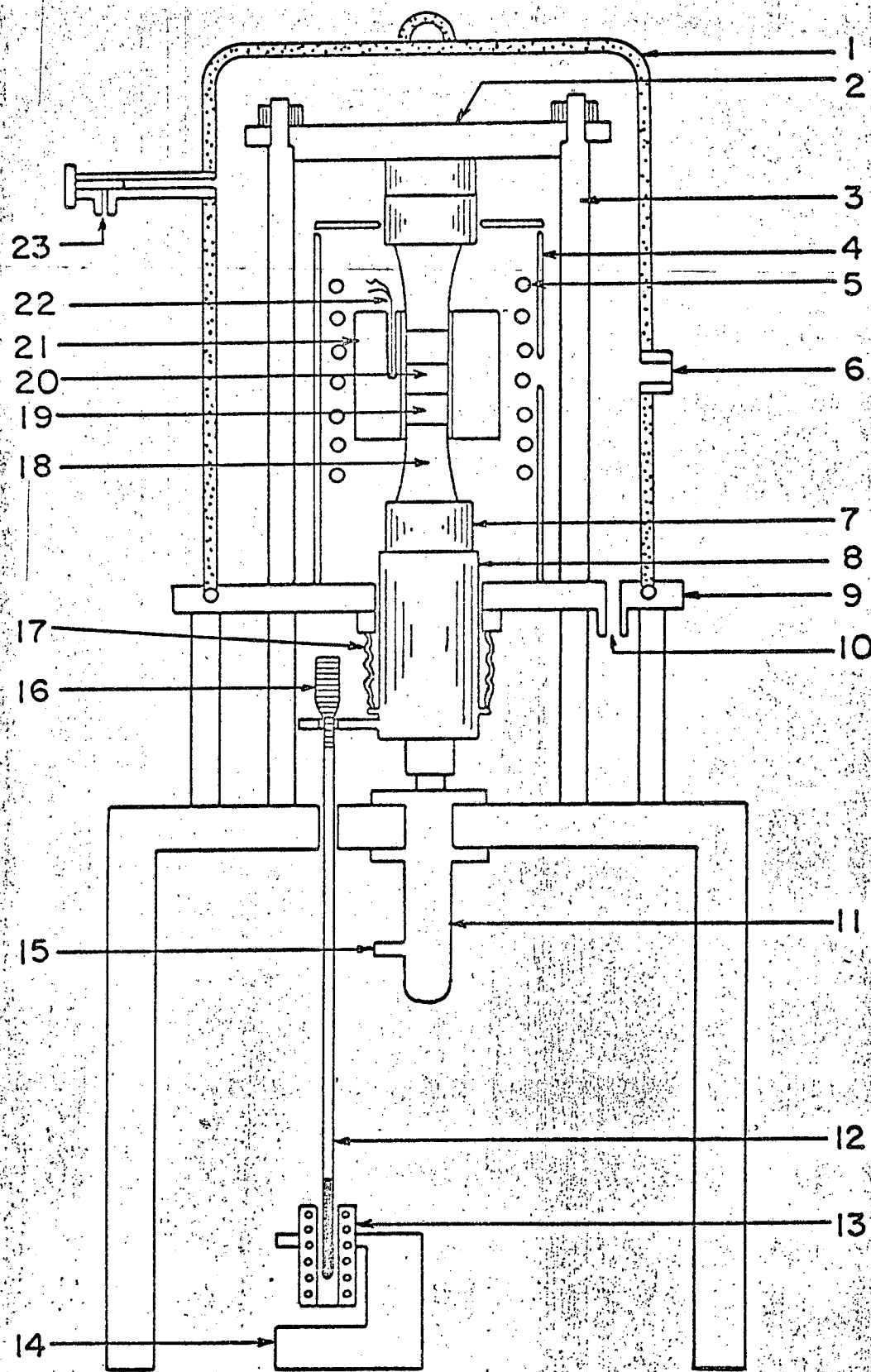

Fig. 1

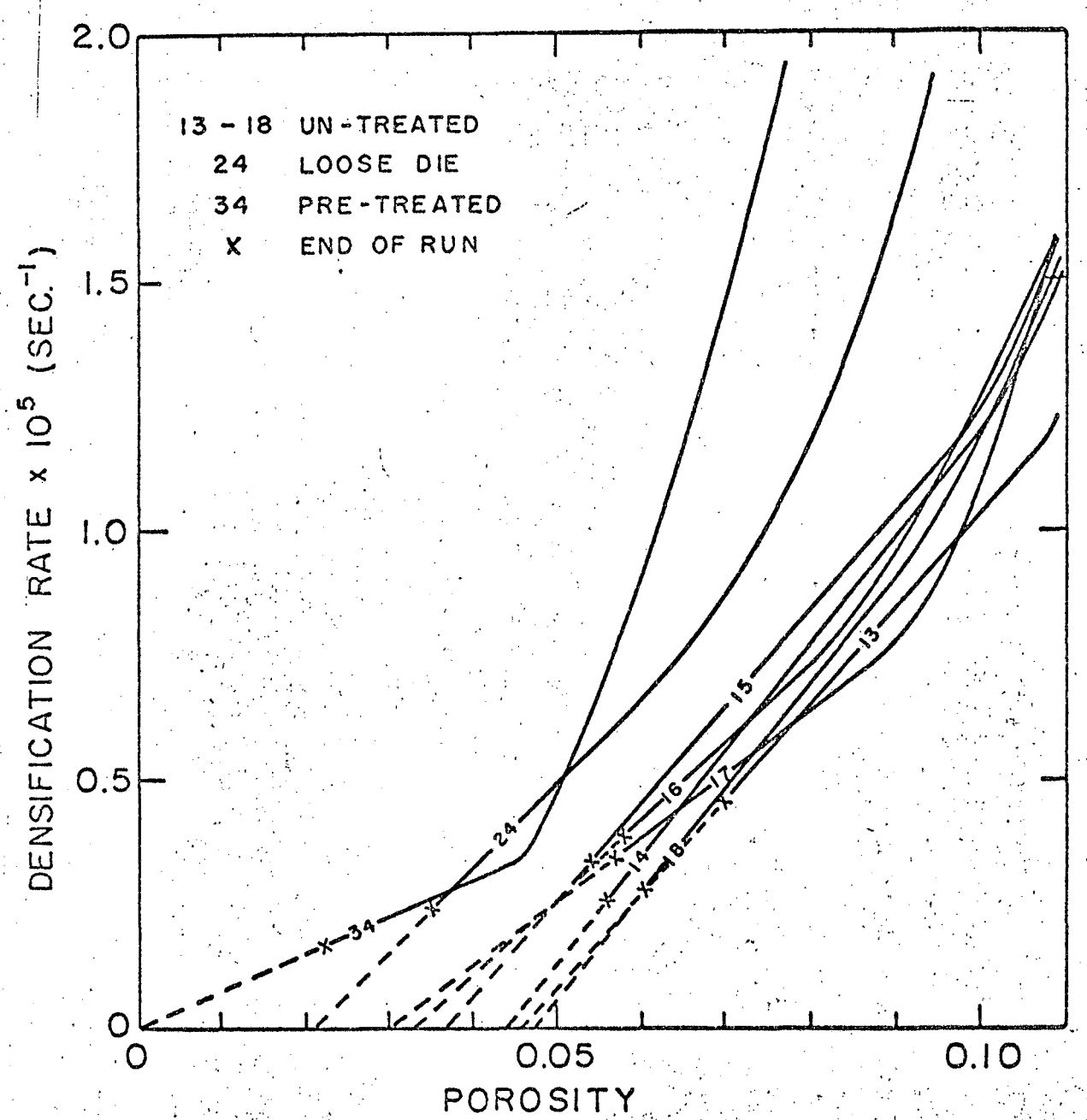
13 - 18 UN-TREATED
24 LOOSE DIE
34 PRE-TREATED
X END OF RUN
DENSIFICATION RATE x 10^5 (SEC.^-1)
2.0
1.5
1.0
0.5
0
0
0.05
0.10
POROSITY
24
34
15
16
17
14
18
13

Fig. 2

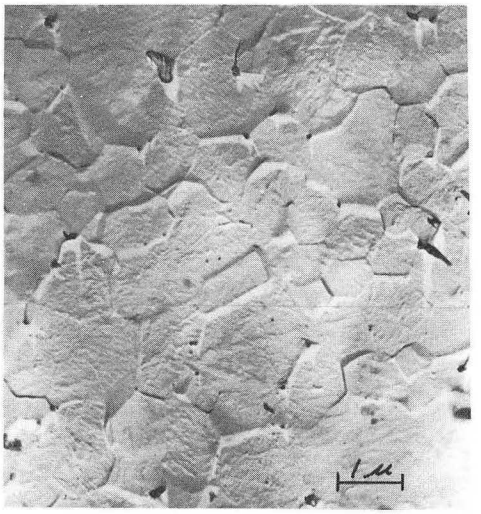

24

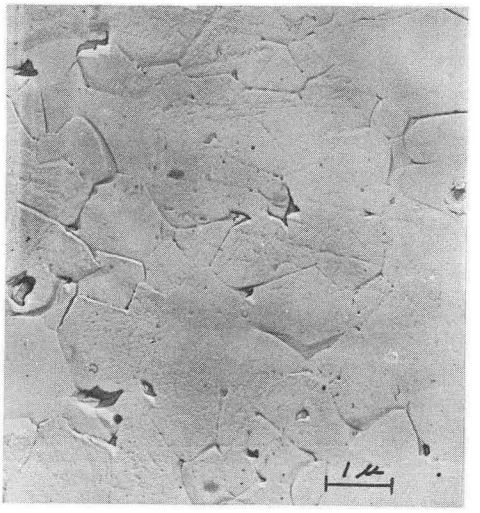

34

ZN-4415

Fig. 3

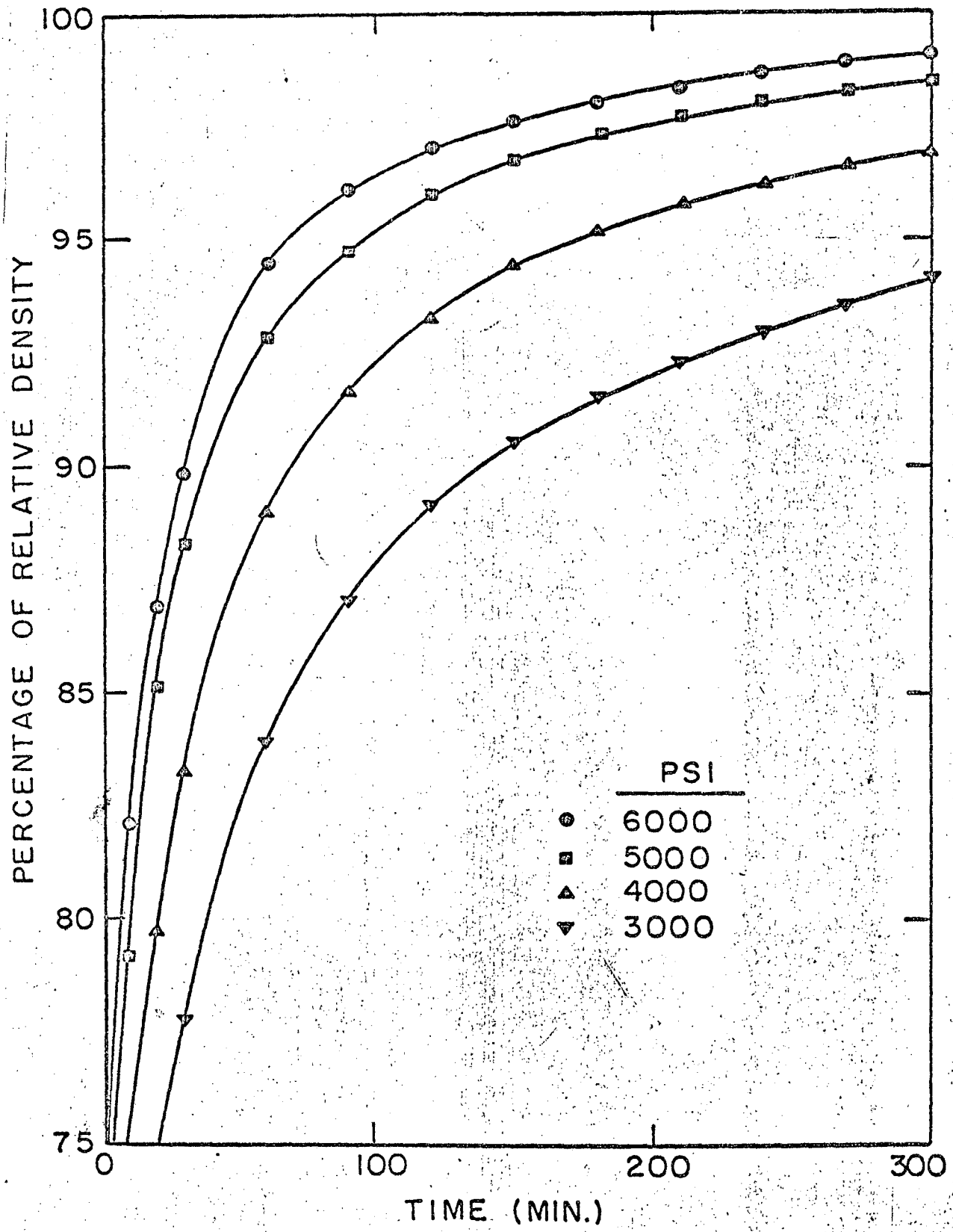
100
95
90
85
80
75
PERCENTAGE OF RELATIVE DENSITY
0
100
200
300
TIME (MIN.)
PSI
6000
5000
4000
3000

Fig. 4

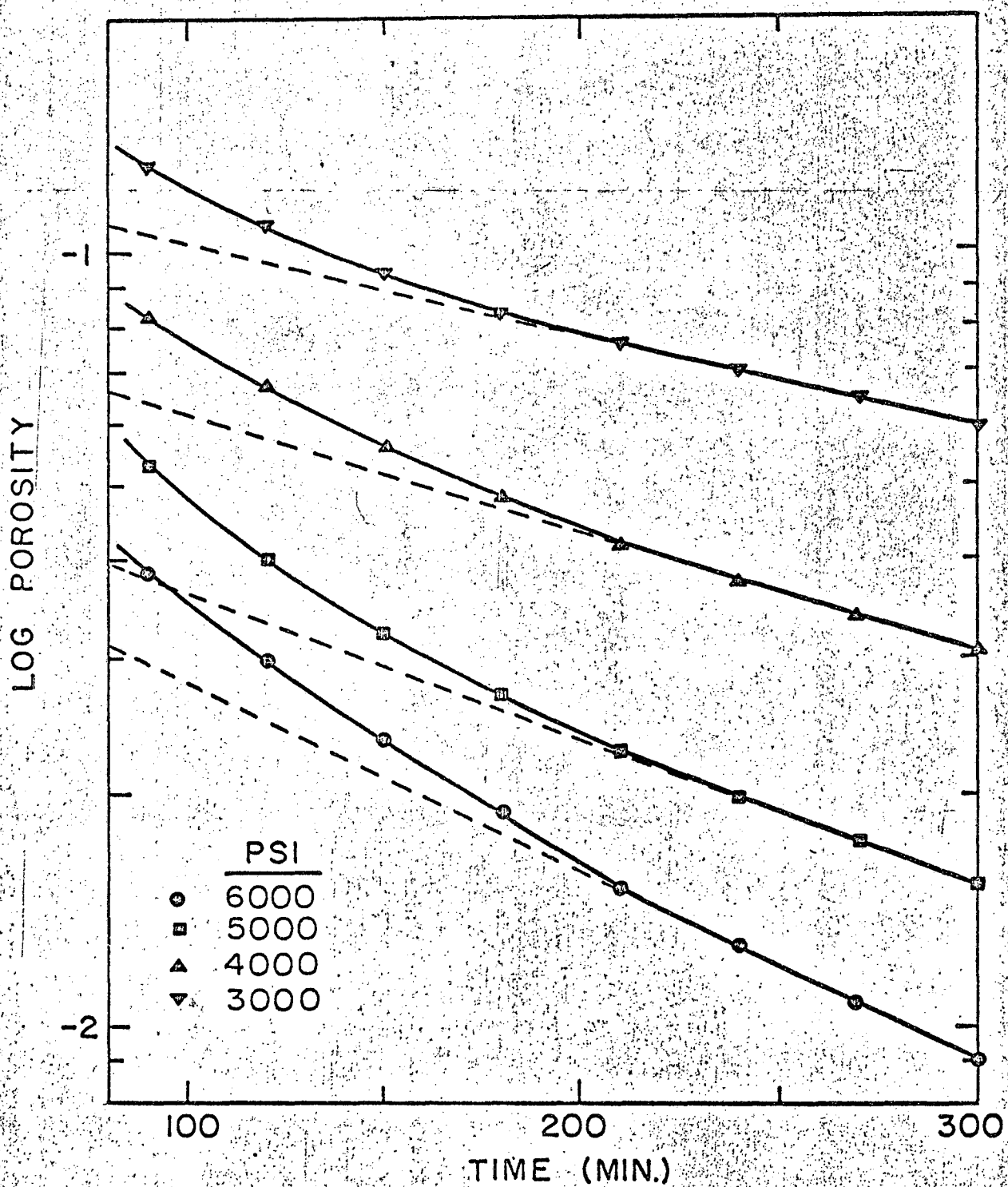

Fig. 5

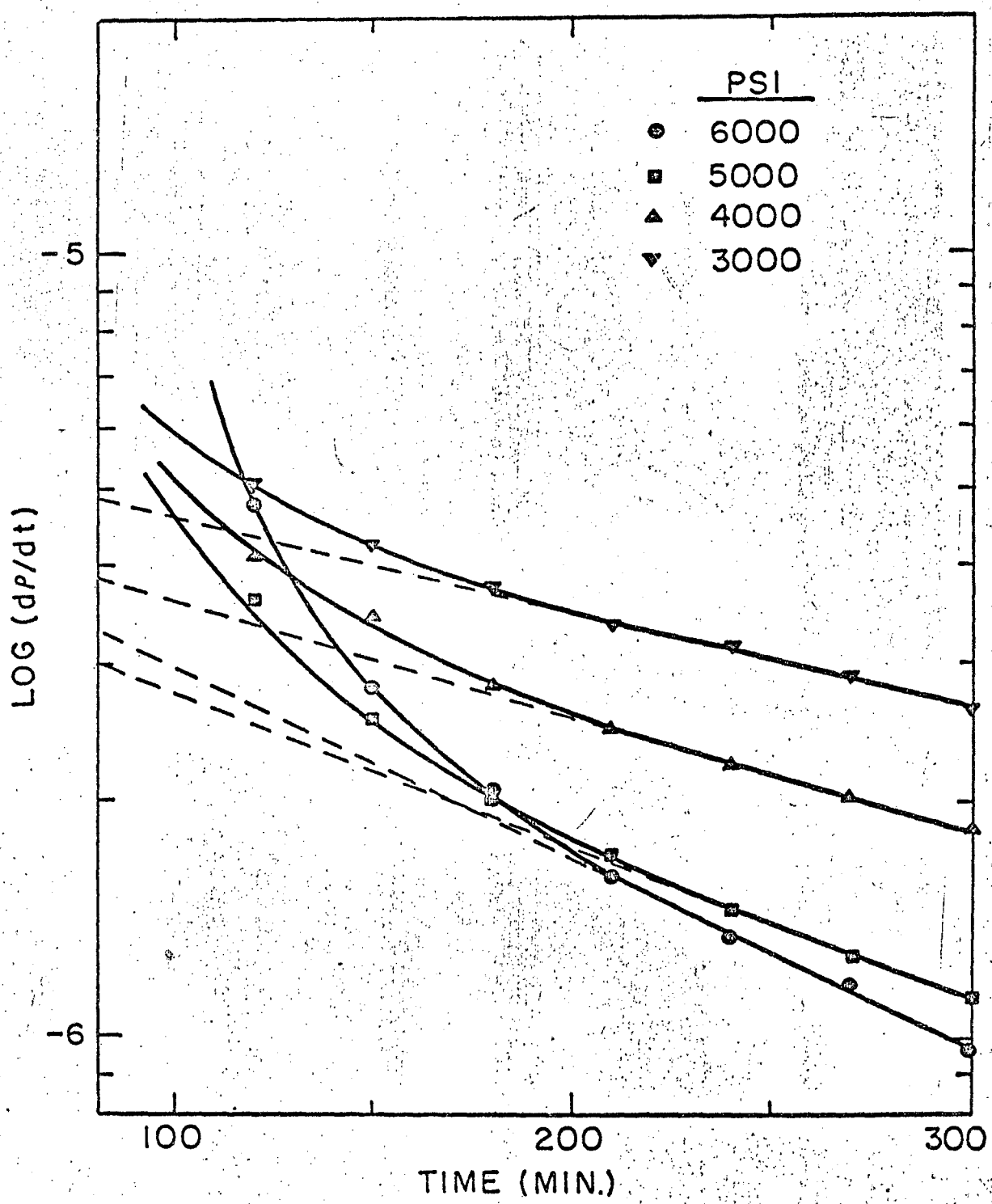

Fig. 6

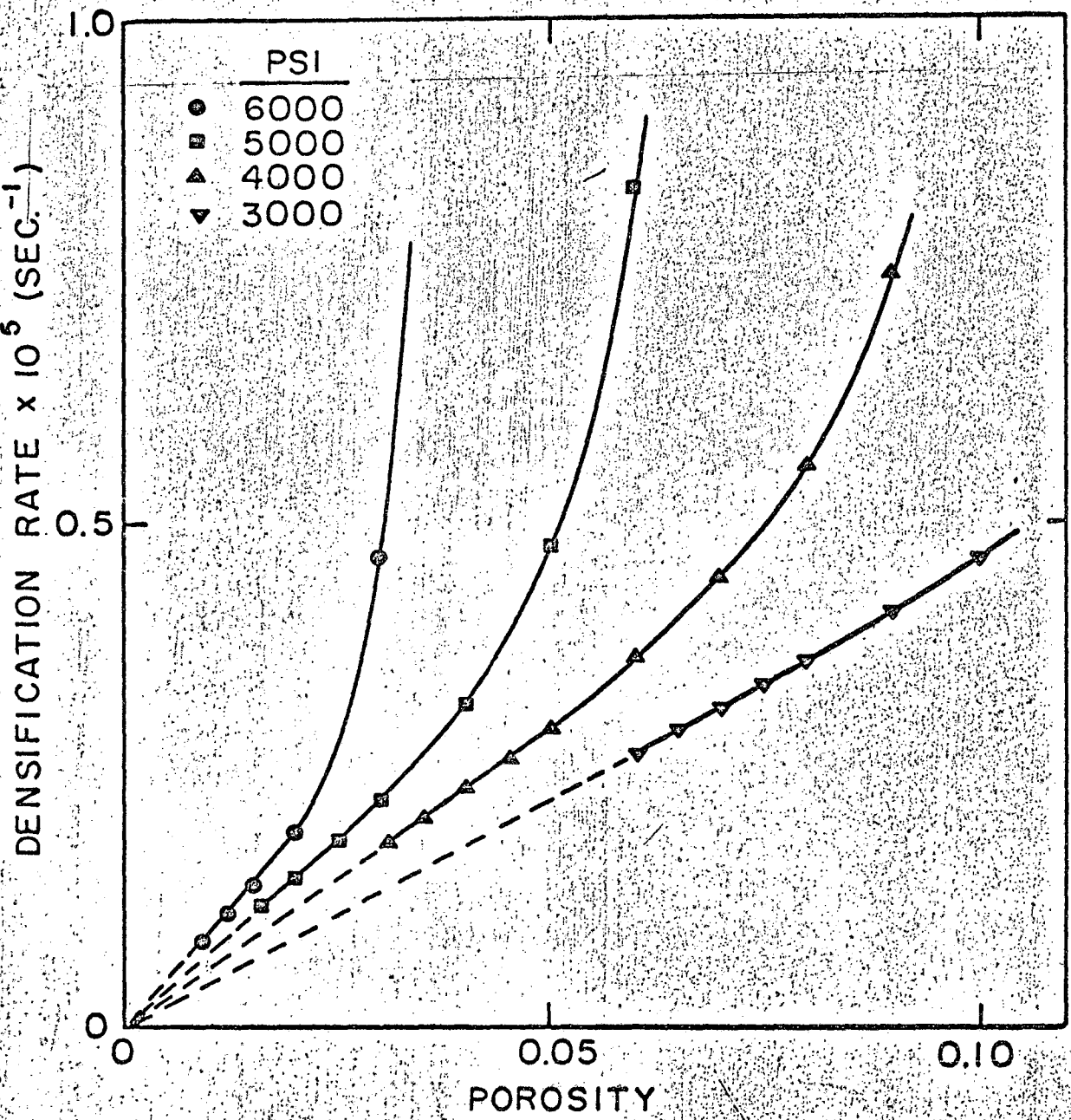
PSI
6000
5000
4000
3000
1.0
0.5
0
DENSIFICATION RATE x 10^5 (SEC.^-1)
0
0.05
0.10
POROSITY

Fig. 7

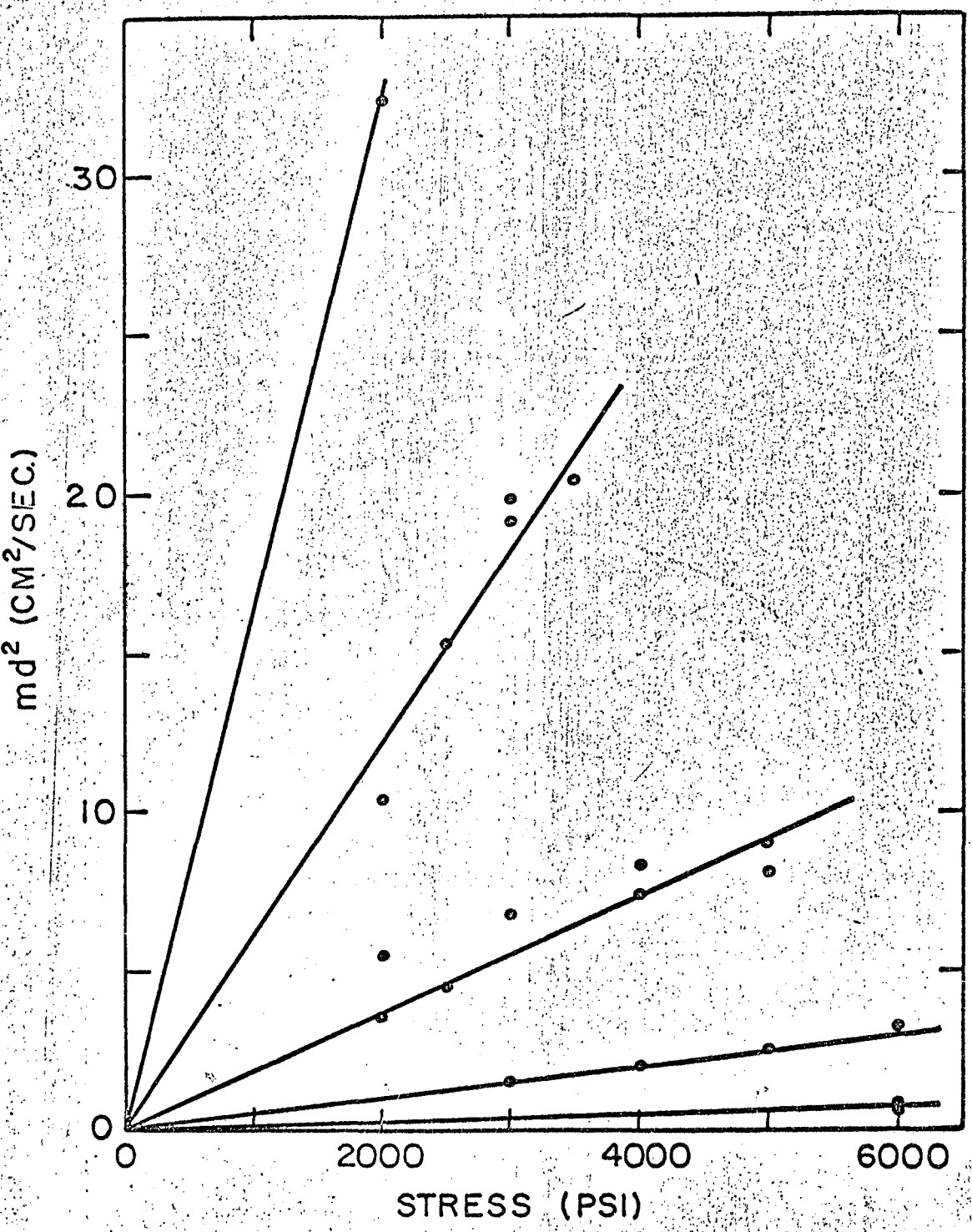

Fig. 8

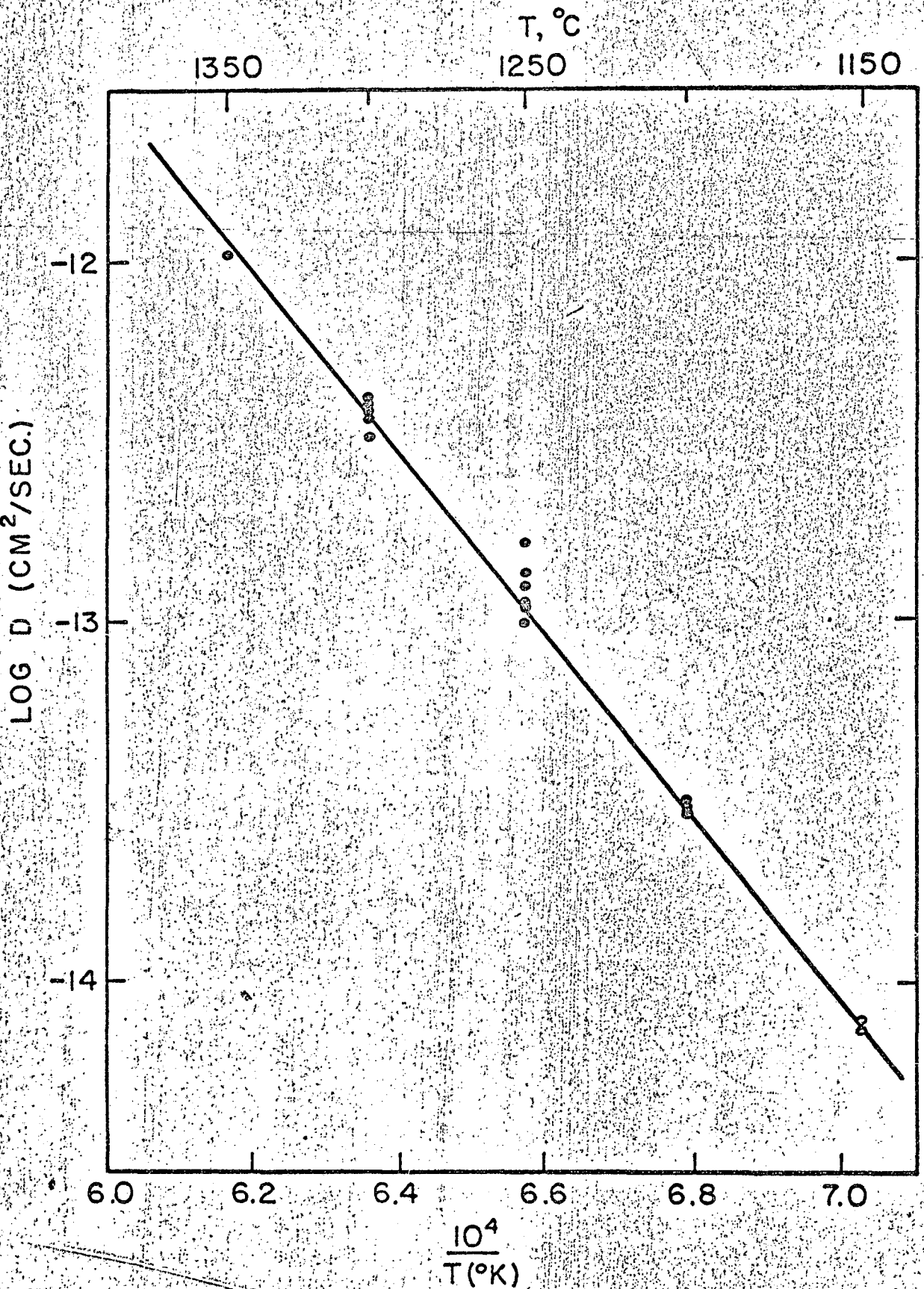

Fig. 9

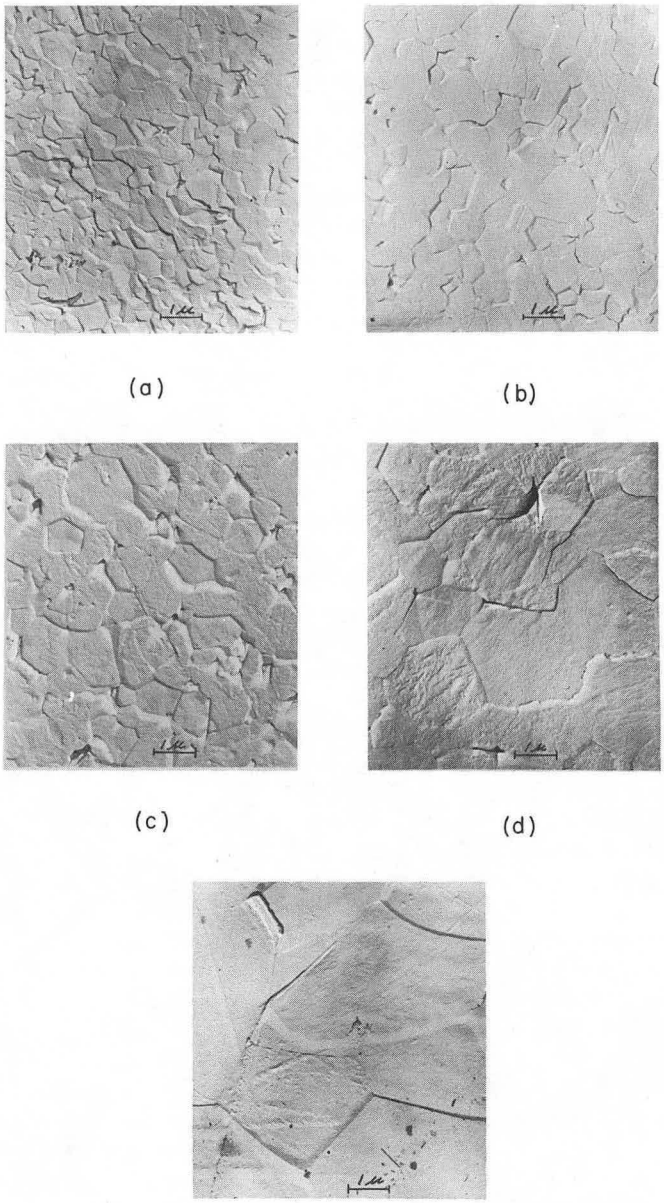

(a) (b) (c) (d) (e)

ZN-4416

Fig. 10

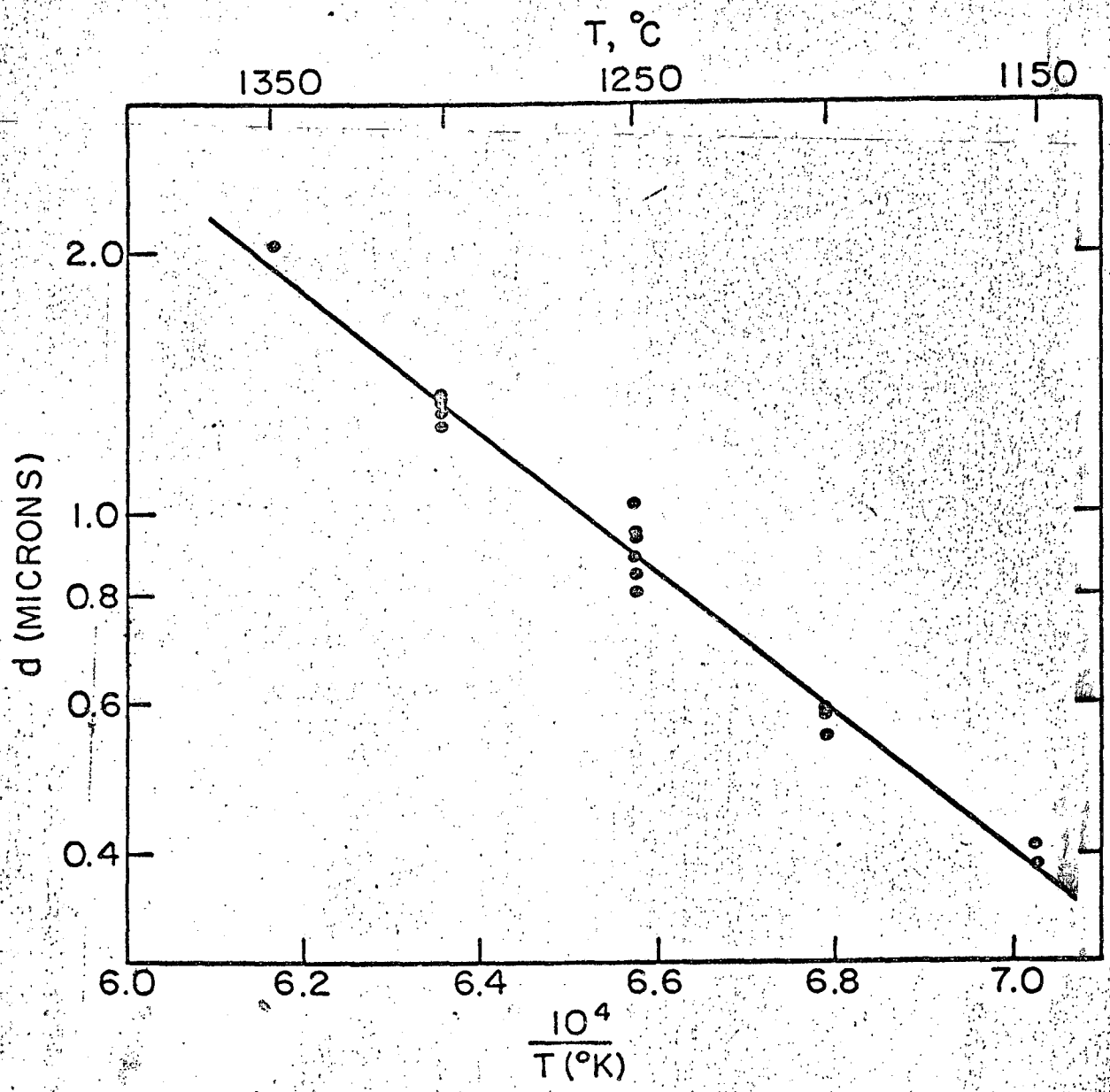

Fig. 11

This report was prepared as an account of Government sponsored work. Neither the United States, nor the Commission, nor any person acting on behalf of the Commission:

A. Makes any warranty or representation, expressed or implied, with respect to the accuracy, completeness, or usefulness of the information contained in this report, or that the use of any information, apparatus, method, or process disclosed in this report may not infringe privately owned rights; or

B. Assumes any liabilities with respect to the use of, or for damages resulting from the use of any information, apparatus, method, or process disclosed in this report.

As used in the above, "person acting on behalf of the Commission" includes any employee or contractor of the Commission, or employee of such contractor, to the extent that such employee or contractor of the Commission, or employee of such contractor prepares, disseminates, or provides access to, any information pursuant to his employment or contract with the Commission, or his employment with such contractor.